Engineering Research Journal
journal homepage: https://erj.journals.ekb.eg/

Numerical and Experimental Investigation of an Evacuated Tube Solar Collector Performance Using Different Nanofluids

Ahmed Yehia[1], Hesham Abd Elmoez[1], Ahmed Mostafa[2,3], Hassan Mohamed[1,*]

[1]Physics and Engineering Mathematics Department, Faculty of Engineering El-Materia, Helwan University, Cairo, Egypt.
[2]Mechanical Power Engineering Department, Faculty of Engineering El-Materia, Helwan University, Cairo, Egypt.
[3]Energy and Renewable Energy Engineering Program, Faculty of Engineering and Technology, Egyptian Chinese University.
*Corresponding Author E-mail: hassan.mohamed@m-eng.helwan.edu.eg

Abstract
Nanofluids are highly effective in enhancing the performance of heat transfer devices due to their high thermal conductivity. Various types of nanoparticles have been utilized, making these nanofluids particularly beneficial for renewable energy applications, such as solar collectors. Evacuated tube solar collector (ETSC) is widely used in thermal applications. This paper presents a study using a mathematical model to evaluate the performance of an ETSC using different nanofluids materials under different climatic conditions in Cairo, Egypt. The mathematical model was validated through experimental tests using water as the working fluid at different flow rates, demonstrating the model's reliability. The study also compared the performance using different nanoparticles (Cu, Ag, and Al_2O_3) at different concentrations. The key findings showed that increasing the volume concentration of hybrid nanoparticles increased the outlet temperature, with Ag yielding the highest temperature increase, followed by Cu, and then Al_2O_3, across various inlet temperatures and flow rates.

Keywords: Numerical, Experimental, Performance, Evacuated Tubes Solar Collector, Nanofluid.

1 Introduction

Renewable energy represents the future, offering environmental benefits and aiding the next generation in producing more power. Solar energy, a crucial type of renewable energy, is harnessed to generate useful heat through solar collectors like flat plate, evacuated tube, parabolic trough, and dish collectors. Significant efforts and investments from researchers and companies have focused on enhancing the efficiency of these collectors. We believe that continued research in this area is essential and anticipate new advancements in the coming years. Eidan et al. (2018) optimized HP-ETSCs with Al_2O_3 and CuO/acetone nanofluids for hot water in the Middle East, finding a 70% filling ratio and 45° tilt angle to be ideal. Nanofluids enhanced thermal performance by 20-54% and efficiency by 15-38%. These results are useful for researchers exploring nanofluids in sunny areas [1].
Sharafeldin and Grof (2018) investigated evacuated tube solar collectors with CeO_2/water nanofluid, showing that higher CeO_2 concentrations led to greater temperature differences and heat gain. This

DOI: 10.21608/erj.2024.308671.1082
Received 31 July 2024; Received in revised form 11 August 2024; Accepted 13 August 2024
Available online 01 September 2024

indicates nanofluids can boost solar collector efficiency by enhancing heat transfer and thermo-optical properties [2].

Ozsoy and Corumlu (2018) experimentally analyzed a thermosyphon heat pipe evacuated tube solar collector using silver-water nanofluid, demonstrating a significant thermal efficiency boost (20.7-40%) compared to pure water. The nanofluid maintained superior heat transfer properties over time, proving its suitability for long-term commercial use [3]. Gan *et al.* (2018) studied TiO_2 nanofluid's impact on ETSC performance, discovering that optimized nanofluid improved thermal conductivity by 7.28%, increased efficiency by 16.5%, and decreased entropy generation by 1.23%. The findings highlight the potential of high thermal conductivity nanofluids to enhance ETSC efficiency [4].

Sharafeldin and Gróf (2019) examined the effect of WO_3/water nanofluid on evacuated tube solar collectors, finding a 21% increase in temperature differences and a 23% boost in heat gain. Their results achieved a thermal-optical efficiency of 72.8%, highlighting the nanofluid's effectiveness in improving solar collector performance [5]. Sharafeldin *et al.* (2019) evaluated the impact of copper nanofluid on evacuated tube solar collectors, discovering that 0.03% concentration increased temperatures by 51.5% and reduced collector area by 34%. The improved heat removal factor highlights copper nanoparticles' effectiveness in enhancing energy efficiency and lowering CO_2 emissions in solar collector systems [6].

Radwan *et al.* (2019) tested evacuated tube heat pipe solar collectors with Al_2O_3/water nanofluid in Cairo's climate, finding that a 45° tilt angle provided optimal performance. They observed up to a 49% increase in thermal efficiency with higher nanofluid concentrations, highlighting the potential for improved collector efficiency and heat gain in building heating applications [7]. Yurddaş (2020) optimized evacuated tube solar collectors (ETSCs) with different nanofluids, notably $Cu - H_2O$, which enhanced thermal performance. Numerical analysis revealed improved heat transfer with higher nanoparticle concentrations, longer tubes, and smaller tank diameters. The study highlights the potential of nanofluids in creating efficient, pollution-free solar energy systems [8].

Eltaweel *et al.* (2020) conducted experiments on a heat pipe evacuated tube solar collector using MWCNT/water nanofluids, analyzing energy and exergy efficiencies. They found that increasing flow rates and nanofluid concentrations improved efficiency, with peak values of 55% for energy efficiency and 10% for exergy efficiency achieved with 0.05 wt% MWCNT/water nanofluid [9]. Hosseini and Dehaj (2021) assessed TiO_2 nanofluids with various morphologies in a U-type evacuated tube solar collector. They found that TiO_2 nanowires improved thermal conductivity by 12.4%, outperforming TiO_2 nanoparticles. The efficiency of the collector increased by up to 21.1% with nanowires and 12.2% with nanoparticles at a flow rate of 0.5 L/min, while pressure drops were affected by viscosity and flow rate [10].

Özcan *et al.* (2023) examined U-pipe evacuated tube solar collectors using TiO_2/water nanofluid, finding an efficiency increase of up to 22.1%, though this also led to a higher pressure drop. While TiO_2/water nanofluid improved collector performance, it also raised the pressure drop, and long-term stability of the nanofluid was a notable issue [11]. Elmaboud *et al.* (2019) used Mathematica software to explore the application of gold nanoparticles (GNPs) in cancer treatment via peristaltic blood flow in physiological vessels. Their study showed that GNPs improved temperature distribution, which could aid in cancer therapy, and also offered insights into fluid dynamics under peristaltic conditions [12]. Azadian *et al.* (2019) performed a two-dimensional numerical simulation of U-shaped vacuum tube solar collectors using Flex PDE software and the finite element method. They evaluated one U-type and two U-type collector models, concluding that increasing the number of U-type tubes improved collector efficiency [13]. Mercan and Yurddaş (2019) used ANSYS-Fluent and the Finite-Volume-Method to analyze nanofluids in evacuated tube solar collectors (ETSCs). Their research demonstrated that CuO/H_2O nanofluid significantly improved heat transfer in ETSC systems compared to water alone, with various parameters and angles in the collector design confirming these enhancements [14].

These studies explore non-Newtonian fluid behavior in corrugated channels. The first study examines Jeffrey fluids under electromagnetohydrodynamic conditions, analyzing how wall corrugations and porous media affect velocity and flow resistance. The second study focuses on entropy generation in

micropolar fluids with convective boundary conditions and slip flow, noting that corrugation amplitude and heat transfer coefficient impact entropy generation. Both emphasize the importance of understanding these fluid dynamics for optimizing engineering applications[15-16]. In numerical studies investigate the heat transfer characteristics of nanofluids [17-20]. The two main strategies used to model the flow of nanofluids are the single-phase and two-phase models. While the Single-Phase Model (SPM) has predominantly been utilized to research the heat transfer properties of nanofluids, the two-phase model provides a better understanding of the function of both the fluid phase and solid particles in heat transfer mechanisms.

2 Methodology

This section will provide a detailed discussion of the mathematical model to compare the performance of the collector with various nanofluids by calculating useful heat for each tube and substitution in a group of partial differential equations. The properties of thermophysical properties between water as a base fluid and nanoparticles can be clarified as in Table 1.

Table 1 Thermophysical properties between water as a base fluid and nanoparticles

Physical Properties	H_2O	Cu	Ag	Al_2O_3
$\rho(Kg/m^3)$	997.1	8933	1500	3971
$c_p(J/kgK)$	4179	385	235	765
$k(W/mK)$	0.613	401	249	40
$\sigma(s/m)$	0.05	5.96×10^7	3.6×10^7	1×10^{-5}

2.1 Modelling of solar radiation

Solar radiation intensity, S, is an important parameter affecting ETSC performance. It can be calculated on a surface tilted at angle, ψ, as follows [21],

$$S = S_B R_B + S_{di}\left(\frac{1+cos\,\psi}{2}\right) + \left((S_B + S_{di})\,\vartheta_g\left(\frac{1-cos\,\psi}{2}\right)\right) \quad (1)$$

Where S denotes solar radiation intensity (W/m^2), R_B denotes beam radiation tilt factor (dimensionless), S_B denotes beam radiation incidence on a horizontal surface (W/m^2), S_{di} denotes sky diffuse radiation (W/m^2), ψ denotes tilt angle (degree), ϑ_g denotes diffuse radiation reflectivity (dimensionless). These parameters are calculated as follows,

$$S_B = S_{Bn} * sin\,\alpha \quad (2)$$

Where α denotes solar altitude angle (degree), S_{Bn} denotes beam radiation at normal incidence and is calculated as follows [21],

$$S_{Bn} = A\,e^{-B/sin\alpha} \quad (3)$$

$$sin\,\alpha = (sin\,l * sin\delta) + (cos\,\omega * cos\,l * cos\,\delta) \quad (4)$$

$$R_B = \frac{(cos\,\omega * cos(l-\psi) * cos\,\delta) + (sin(l-\psi) * sin\,\delta)}{(cos(l) * cos\,\omega * cos\,\delta) + (sin(l) * sin\,\delta)} \quad (5)$$

$$S_{di} = C * S_{Bn} * I_{ss} \quad (6)$$

Where A denotes solar radiation at zero air mass (dimensionless),B denotes atmospheric extinction coefficient (dimensionless), C denotes diffuse radiation factor (dimensionless), l denotes latitude angle (degree), δ denotes declination angle (degree), I_{ss} denotes angle factor between radiation beam and

evacuated tube surface (dimensionless), h denotes hour angle (degree). These parameters are calculated from the following equations [21],

$$\omega = (12 \pm local\ time(h)) * 15^0 \quad (7)$$

$$\delta = 23.45\ sin\left(\frac{360}{365} * (284 + n)\right) \quad (8)$$

Where n denotes day number starting from 1 January, S_{di} denotes sky diffuse radiation, is calculated for horizontal surface according to Eq. (6) and the angle factor, I_{ss} denotes equal to unity for horizontal surfaces, while ϑ_g denotes diffuse reflectivity, and is assumed to be 0.2 when there is no snow on the ground [21].

2.2 Radiation incident on a single evacuated tube

According to Tang *et al.* [22] assumptions, the collectable radiation incidence on a tube can be divided into two parts: beam radiation incident directly on the tube, $S_{B,e}$, and diffuse radiation intercepted by the tube, $S_{di,e}$. Instantaneous total radiation incident on a single tube, S_e, is calculated as follows:

$$S_e = S_{B,e} + S_{di,e} \quad (9)$$

$$S_{B,e} = D_{i,e}\ S_{Bn}\ cos\,\theta\ I(\Omega) \quad (10)$$

$$S_{di,e} = D_{i,e}\ \pi\ \left(\frac{1 + cos\,\psi}{2}\right)\ f_{ts}\ S_{di} \quad (11)$$

Where $D_{i,e}$ denotes inner diameter of the evacuated tube (mm), θ denotes angle between the solar ray and its projection on the tube surface (degree), f_{ts} denotes tube-sky shape factor (dimensionless), $I(\Omega)$ denotes angular acceptance function (dimensionless). Can be calculated according to [22],

2.3 Solar energy incidence on ETSC

After the calculation of the instantaneous solar power collected by a single tube, the total instantaneous radiation incident on the ETSC [22],

$$S_{sc} = S_e\ N\ L_e \quad (12)$$

Where S_{sc} denotes total instantaneous radiation incident on the ETSC (W), N denotes number of evacuated tubes (dimensionless), L_e denotes length of the evacuated tube (mm).

2.4 Evacuated tube modelling

To investigate the performance of a single evacuated tube, solar power is transferred to the ETSC through the evacuated tubes. Water is heated and rises to the storage tank by natural convection. Budihardjo and Morrison [23] developed a relation for evaluating the flow rate of natural convection between the storage tank and the evacuated tube heat pipe from Reynolds number, Re, as follow,

$$Re = 0.1914\left(\frac{Nu\ Gr}{Pr} * cos\,s * \left(\frac{L_e}{D_{i,e}}\right)^{1.2}\right)^{0.4084} \quad (13)$$

Where Re denotes Reynolds number (dimensionless), Nu denotes Nusselt number (dimensionless), Pr denotes Prandtl number (dimensionless), Gr denotes Grashof number (dimensionless).

Ren and Zhang [23] studied experimentally the natural convection in a semi-closed cavity and developed a relation for natural convection, which is modified to the following relation,

$$Nu = 0.82\left(Pr\frac{g * sin\,\psi * \beta * S_{sc} * {D_{i,e}}^4}{k_w * \upsilon^2 * L_e * D_{i,e} * \pi * N} * \left(\frac{L_e}{D_{i,e}}\right)^{-3.4}\right)^{0.2} \quad (14)$$

Where g denotes gravity acceleration (m/s^2), β denotes thermal expansion (K^{-1}), k_w denotes thermal conductivity (W/m.℃), υ denotes kinematic viscosity (m^2/s). The heat transfer coefficient, h_e, and the mass flow rate, $\dot{m}_e$, from the tube are calculated by [24],

$$h_e = \frac{Nu * k_w}{D_{i,e}} \quad (15)$$

$$\dot{m}_e = \frac{Re * \pi * \mu * D_{i,e}}{4} \quad (16)$$

Where h_e denotes heat transfer coefficient in the evacuated tube ($W/m^2.$℃), $\dot{m}_e$ denotes mass flow rate from the evacuated tube to the storage tank (kg/sec).Then, the outlet temperature of the pipe, $T_{out,e}$, the temperature of absorber coating, $T_{abs,e}$ and heat losses from the evacuated tube, $\dot{Q}_{l,e}$, are calculated by,

$$T_{out,e} = T_{in,e} + \frac{\dot{Q}_{u,e}}{\dot{m_e} * c_p} \quad (17)$$

$$T_{abs,e} = T_{avg,e} + \frac{\dot{Q}_{u,e}}{\pi\, D_{i,e}\, h_e\, L_e} \quad (18)$$

$$\dot{Q}_{l,e} = h_{rad} * \pi * D_{i,e} * L_e * \left(T_{abs,e} - T_{amb}\right) \quad (19)$$

The useful heat transfer, $\dot{Q}_{u,e}$, can be,

$$\dot{Q}_{u,e} = S_e * L_e - \dot{Q}_{l,e} \quad (20)$$

Where $T_{out,e}$ denotes outlet temperature of the tube (℃), $T_{in,e}$ denotes inlet temperature of the tube (℃), c_p denotes specific heat of water ($j/kg.$℃), $\dot{Q}_{u,e}$ denotes useful heat transfer (W), $T_{abs,e}$ denotes absorbent temperature (℃), $\dot{Q}_{l,e}$ denotes heat losses of the tube (W), h_{rad} denotes radiative heat transfer coefficient ($W/m^2.$℃), T_{amb} denotes ambient temperature (℃).

The tube instantaneous efficiency can be calculated by,

$$\eta_e = \frac{\dot{Q}_{u,e}}{S_e * L_e} = \frac{\dot{m}_e c_p (T_{out,e} - T_{in,e})}{S_e * L_e} \quad (21)$$

The calculation steps are presented in a flow chart as shown in Figure (1) to calculate the amount of useful heat for evacuated tube $\dot{Q}_{u,e}$, and substitution in Governing equations.

2.5 Governing equations

The governing equations are partial differential equations that include the continuity, momentum, and energy equations [25-29].

$$\frac{\partial \rho}{\partial t} + \rho\left[\frac{\partial u}{\partial x} + \frac{\partial v}{\partial y}\right] = 0 \quad (22)$$

$$\rho_{nf}\left(\frac{\partial u}{\partial t} + u\,\frac{\partial u}{\partial x} + v\,\frac{\partial u}{\partial y}\right) = -\left(\frac{\partial p}{\partial x}\right) + \mu_{nf}\left(\frac{\partial^2 u}{\partial x^2} + \frac{\partial^2 u}{\partial y^2}\right) \quad (23)$$

$$\rho_{nf}\left(\frac{\partial v}{\partial t} + u\,\frac{\partial v}{\partial x} + v\,\frac{\partial v}{\partial y}\right) = -\left(\frac{\partial p}{\partial y}\right) + \mu_{nf}\left(\frac{\partial^2 v}{\partial x^2} + \frac{\partial^2 v}{\partial y^2}\right) \quad (24)$$

$$\left(\rho c_p\right)_{nf}\left(\frac{\partial T}{\partial t} + u\frac{\partial T}{\partial x} + v\frac{\partial T}{\partial y}\right) = k_{nf}\left(\frac{\partial^2 T}{\partial x^2} + \frac{\partial^2 T}{\partial y^2}\right) + Q_{rad} + Q_{Tank} \quad (25)$$

When the water flow rate is constant, the velocity in the x-direction (u) is zero, and there is no motion in the y-direction, making the velocity (v) zero as well. Since the system operates under atmospheric pressure, both $\left(\frac{\partial p}{\partial x}\right)$ and $\left(\frac{\partial p}{\partial y}\right)$ are zero. Consequently, the continuity and momentum equations are zero, and the energy equation simplifies to:

$$\left(\rho c_p\right)_{nf}\left(\frac{\partial T}{\partial t}\right) = Q_{rad} + Q_{Tank} \tag{26}$$

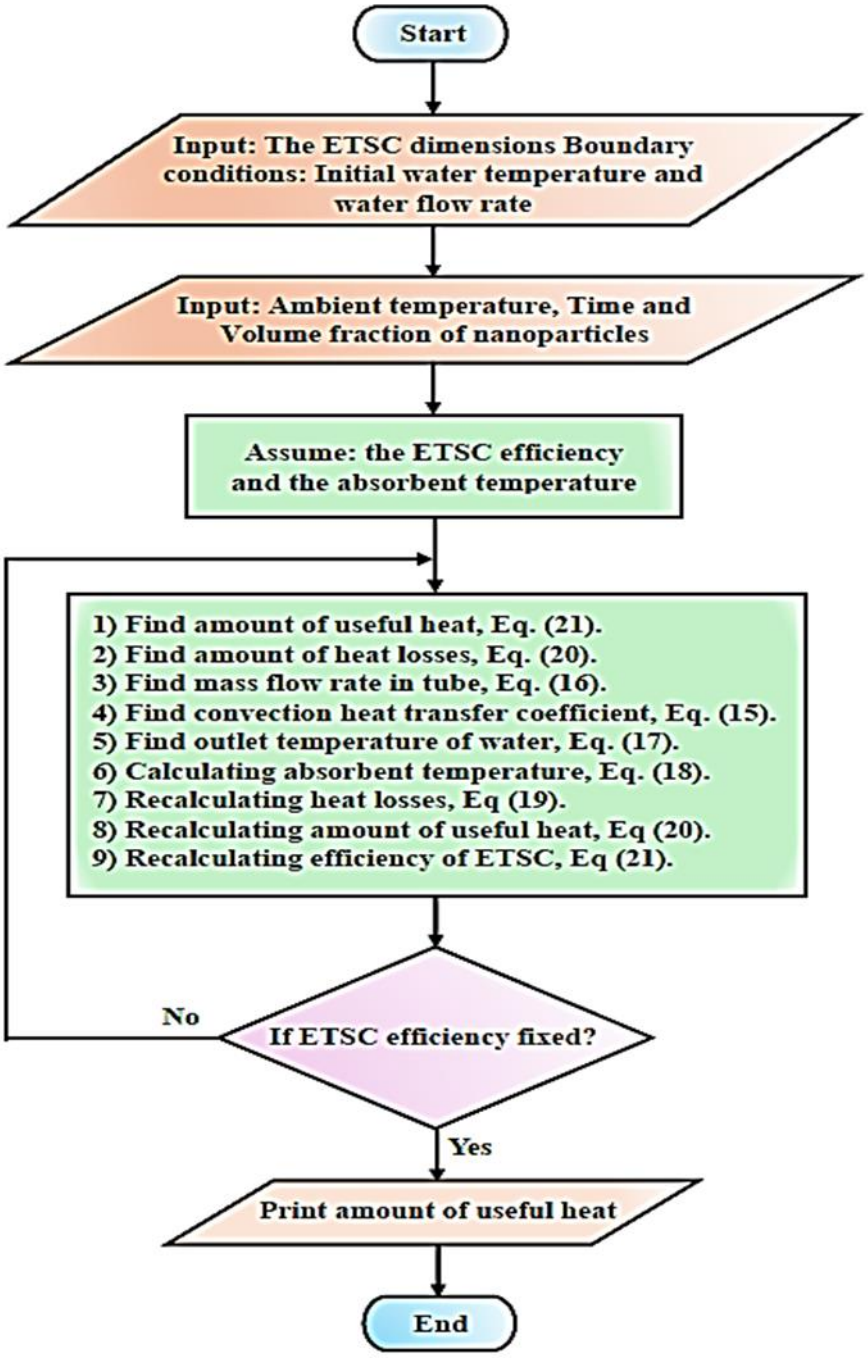

Fig. 1. Steps of the Computational Model.

Using the energy equation, we can determine the outlet temperature from a single tube. By applying this calculation 30 times, we can then find the outlet temperature for the entire evacuated tube solar collector.
To verify the accuracy of this model, it is validated against an experimental model using water as the working fluid.

3 Test Rig Description

Figure (2) show a schematic diagram of the test rig used to study experimentally the performance evaluation of evacuated tubes solar collector with nanofluids under different climate conditions in Egypt.

3.1 Test Procedure

The city water is opened to fill the tank, When the water reaches a certain level, the ball valve for the inlet of evacuated tubes solar collector is opened while the by-pass ball valve is closed and the circulation pump is turned on to pumped water into the evacuated tubes solar collector, and the evacuated tubes solar collector outlet valve is opened until the tank of evacuated tubes solar collector is filled. The system runs until steady-state conditions are reached, then, the flow rate is adjusted by controlling the openings of the inlet ball valve and the by-pass ball valve, while controlling the water temperature inlet the evacuated tubes solar collector using the electric heater and the cooling coil. Subsequently, the temperatures of the water entering and exiting the evacuated tubes solar collector and flow rate are measured and recorded.

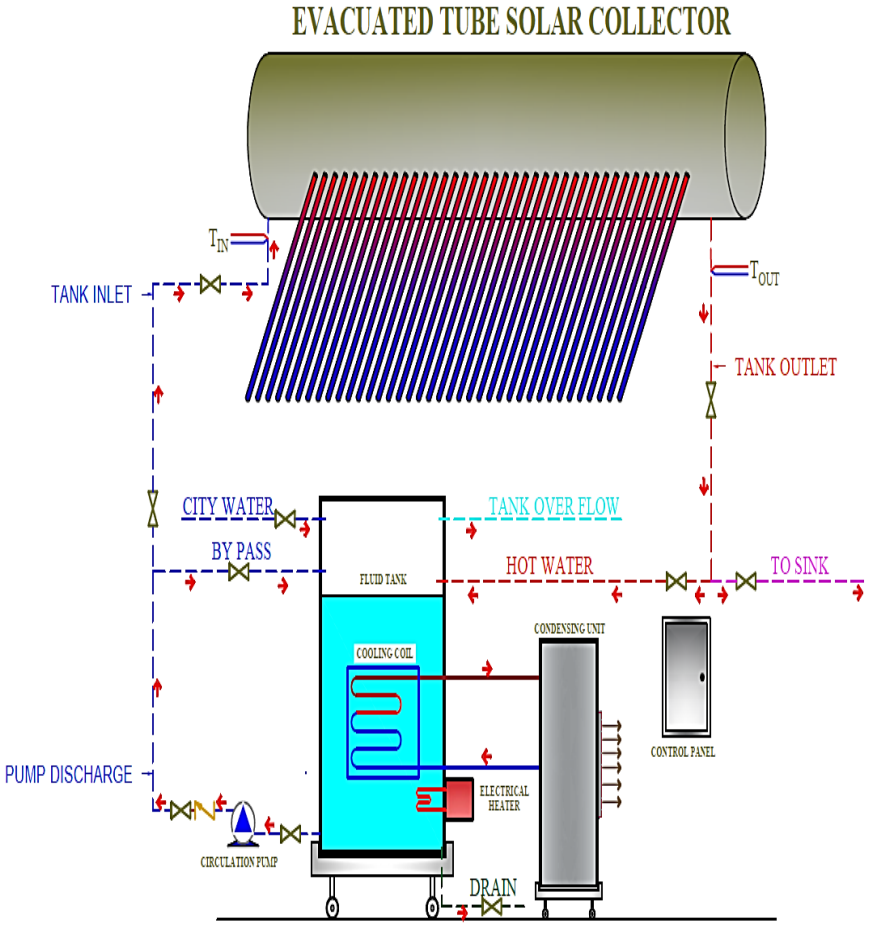

LEGEND	
SYMBOL	DISCRIPTION
⋈	BALL VALVE
N	NON- RETURN VALVE
	CIRCULATION PUMP
	THERMO COUPLE K-TYPE

K-TYPE THERMO COUPLE	
ABBERVIATION	DISCRIPTION
T_{IN}	EVACUATED TUBE SOLAR COLLECTOR INLET TEMPERATURE
T_{OUT}	EVACUATED TUBE SOLAR COLLECTOR OUTLET TEMPERATURE

Fig. 2. Schematic diagram of experimental test rig.

3.2 Model Validation

Where flow rate is 0.05 kg/sec As shown Figure (3) The outlet temperature on $15/9/2022$ ranging [25.7 ℃ – 30.9 ℃] experimentally and [26.87 ℃ – 31.62 ℃] mathematically at average temperature entering the solar collector is 25.07 ℃, and the error rate between the two results is 4.67%. The outlet temperature on $5/9/2022$ ranging [33.1 ℃ – 37.4 ℃] experimentally and [31.7 ℃ – 36.47 ℃] mathematically at average temperature entering the solar collector is 30.06 ℃, and the error rate between the two results is 2.08%.

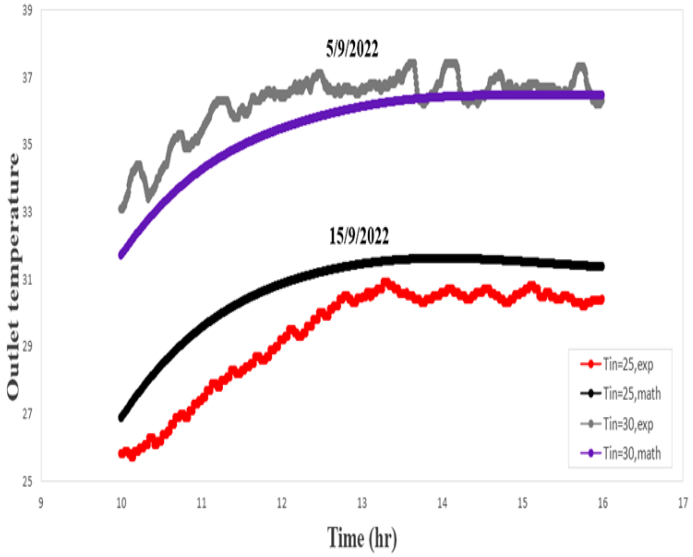

Fig. 3. Water outlet temperature (5/9/2022) & (15/9/2022).

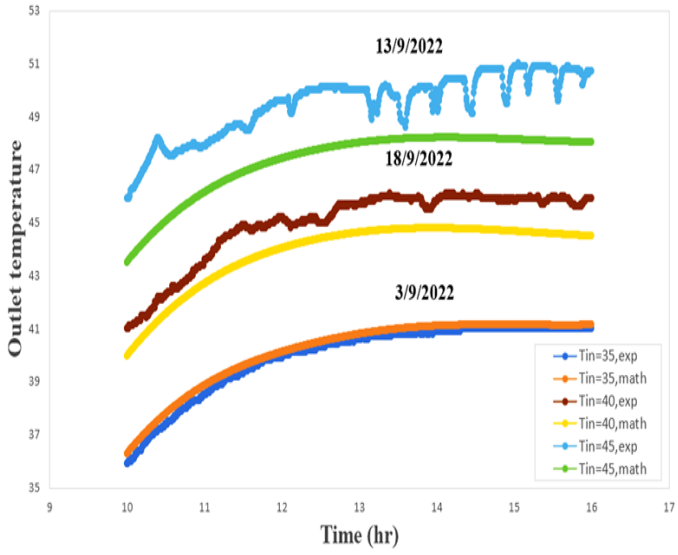

Fig. 4. Water outlet temperature (3/9/2022) & (13/9/2022) & (18/9/2022).

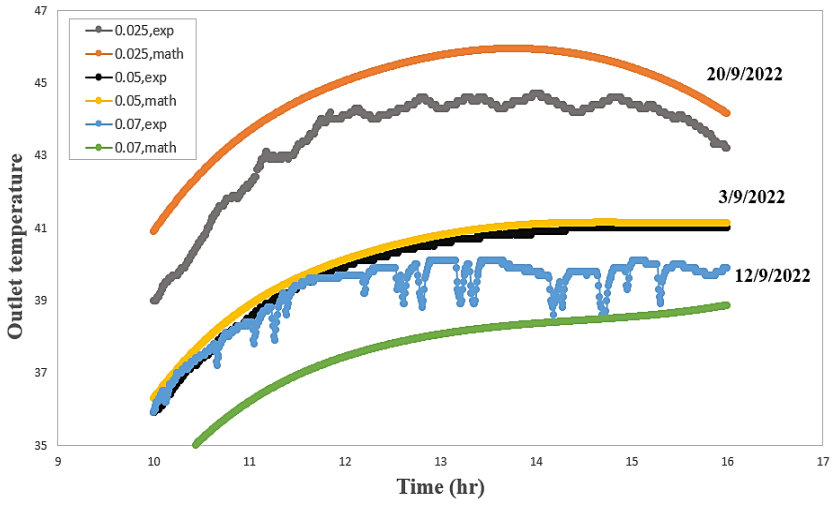

Fig. 5. Water outlet temperature with deferent flow rate.

As shown in Figure (4) at 0.05 kg/sec flow rate The outlet temperature on $5/9/2022$ ranging [35.9 ℃ – 41.1 ℃] experimentally and [36.29 ℃ – 41.15 ℃] mathematically at average temperature entering the solar collector is 35.29 ℃, and the error rate between the two results is 0.55%. The outlet temperature on $18/9/2022$ ranging [41 ℃ – 46.1 ℃] experimentally and [39.97 ℃ – 44.79 ℃] mathematically at average temperature entering the solar collector is 40.07 ℃, and the error rate between the

two results is 2.34%. The outlet temperature on $13/9/2022$ ranging [45.9 ℃ – 51 ℃] experimentally and [43.51 ℃ – 48.21 ℃] mathematically at average temperature entering the solar collector is 44.44 ℃, and the error rate between the two results is 4.33%.
Figure (5) illustrates the validation at an inlet temperature of 35℃ for different flow rates ($0.025\ kg/sec, 0.05\ kg/sec, 0.07\ kg/sec$). It is concluded that the lowest flow rate yields the highest temperature, while the highest flow rate results in the lowest temperature.
Validating the experimental model against the mathematical model confirms the reliability of the mathematical model.

4 Results and Discussion

Nanoparticles Cu, Ag and Al_2O_3 at volume of 0.03 and 0.06 were mixed with water, analyzed through a computational model, and compared against the performance of pure water.
Figures (6-10) show the temperature of outlet (in degrees Celsius) from an evacuated tube solar collector over time (in hours) on (3, 5, 13, 15, 18/9/2022). The graph includes data for water and various nanofluids with different nanoparticles (Cu, Ag and Al_2O_3) and concentrations (0.03 and 0.06 vol%) at flow rate 0.05 kg/sec.
Figures (6-10) show the temperature of outlet (in degrees Celsius) from an evacuated tube solar collector over time (in hours) on (3, 5, 13, 15, 18/9/2022). The graph includes data for water and various nanofluids with different nanoparticles (Cu, Ag and Al_2O_3) and concentrations (0.03 and 0.06 vol%) at flow rate 0.05 kg/sec and inlet temperature ($25, 30, 35, 40, 45$ ℃).
Figures (11-12) show the temperature of outlet (in degrees Celsius) from an evacuated tube solar collector over time (in hours) on (12, 20/9/2022). The graph includes data for water and various nanofluids with different nanoparticles (Cu, Ag and Al_2O_3) and concentrations (0.03 and 0.06 vol%) at flow rate (0.025 kg/sec and 0.07kg/sec) and inlet temperature 35℃.
All curves exhibit a similar pattern: the outlet fluid temperature rises from around 9 AM, peaks at midday, and then gradually decreases. The nanofluid with 0.06 vol% Ag nanoparticles (blue curve) reaches the highest outlet water temperature, while the 0.03 vol% Ag nanoparticles (cyan curve) also perform well but at a slightly lower temperature than the 0.06 vol% concentration. The 0.06 vol% Cu nanofluid (grey curve) outperforms the 0.03 vol% Cu nanofluid (yellow curve), with the former reaching a higher peak temperature. The 0.06 vol% Al2O3 nanofluid (brown curve) performs better than the 0.03 vol% Al2O3 nanofluid (dark brown curve), but both have lower peak temperatures compared to Ag and Cu nanofluids. Plain water (orange curve) consistently has the lowest outlet temperature throughout the time period.
From the figures, it can be seen that Silver (Ag) nanofluids perform the best in increasing outlet water temperature, followed by copper (Cu) and aluminum oxide (Al_2O_3).

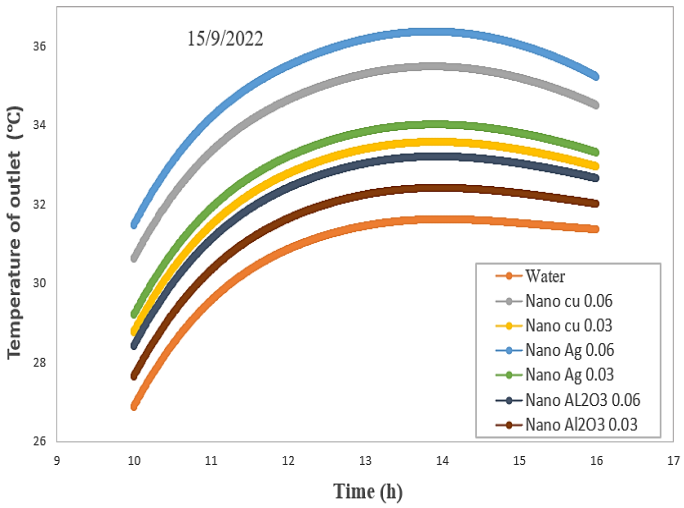

Fig. 6. Water outlet temperature (15/9/2022).

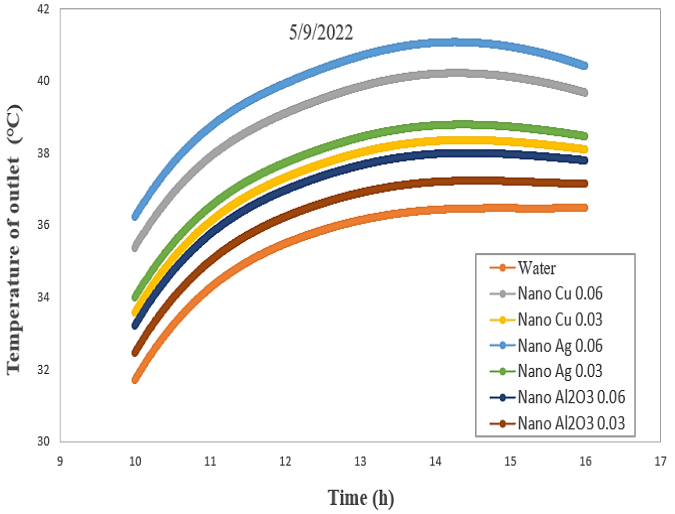

Fig. 7. Water outlet temperature (5/9/2022).

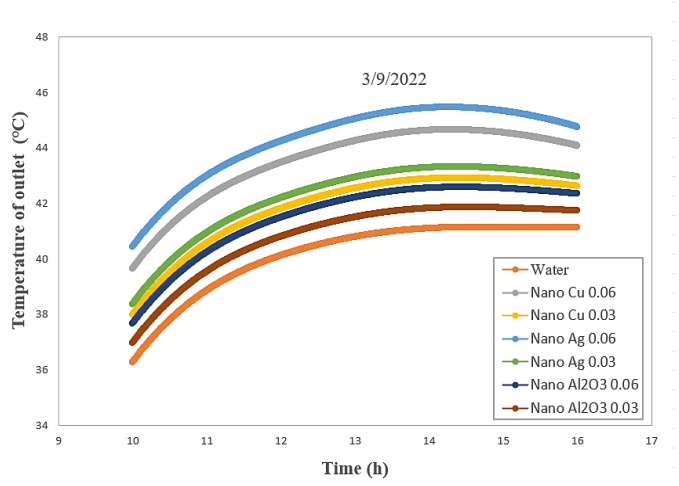

Fig. 8. Water outlet temperature (3/9/2022).

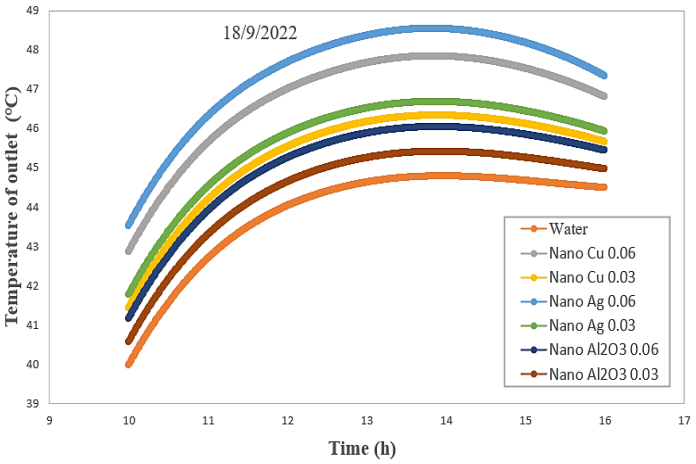

Fig. 9. Water outlet temperature (18/9/2022).

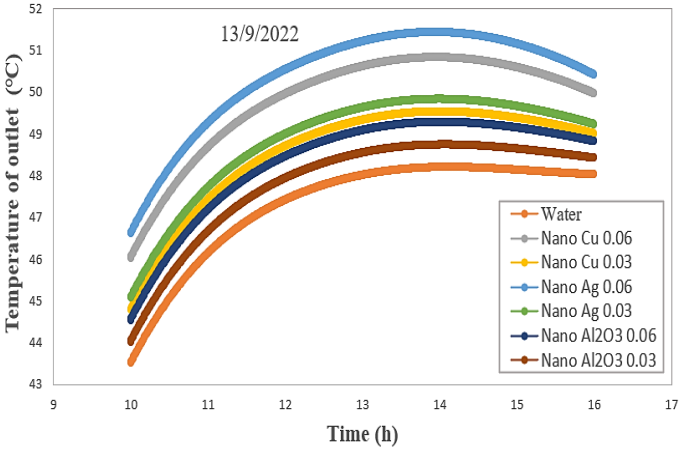

Fig. 10. Water outlet temperature (13/9/2022).

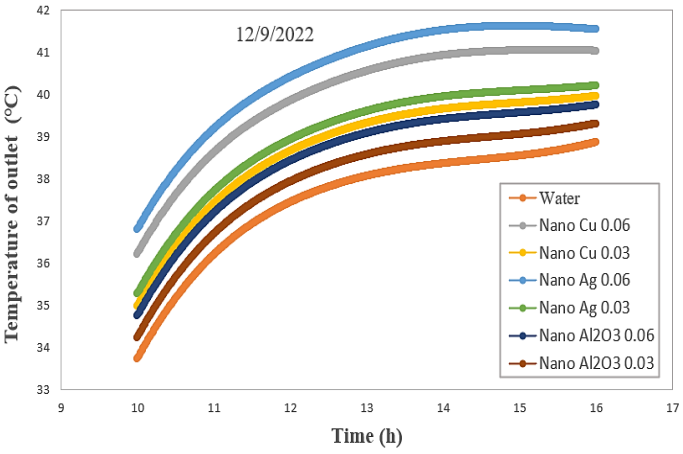

Fig. 11. Water outlet temperature (12/9/2022).

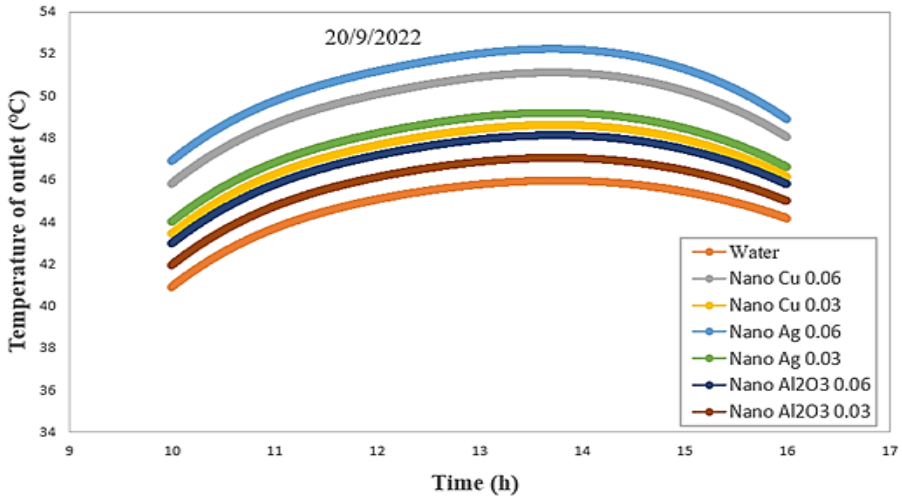

Fig. 12. Water outlet temperature (20/9/2022).

5 Conclusion

Nanofluids, especially at higher concentrations (0.06 vol%), typically result in higher outlet temperatures than at lower concentrations (0.03 vol%). They significantly enhance the thermal performance of evacuated tube solar collectors compared to water alone. Silver (*Ag*) nanofluids perform the best in increasing outlet water temperature, followed by copper (*Cu*) and aluminum oxide (Al_2O_3). These results highlight the potential of nanofluids to improve the efficiency of solar thermal systems, making them more effective for energy applications. The inclusion of nanoparticles greatly boosts the solar collector's thermal performance compared to plain water.

Reference

[1] A. A. Eidan, A. AlSahlani, A. Q. Ahmed, M. Al-fahham, and J. M. Jalil, "Improving the performance of heat pipe-evacuated tube solar collector experimentally by using Al2O3 and CuO/acetone nanofluids," *Sol. Energy*, vol. 173, pp. 780–788, Oct. 2018, doi: 10.1016/j.solener.2018.08.013.

[2] M. A. Sharafeldin and G. Gróf, "Evacuated tube solar collector performance using CeO2/water nanofluid," *J. Clean. Prod.*, vol. 185, pp. 347–356, Jun. 2018, doi: 10.1016/j.jclepro.2018.03.054.

[3] A. Ozsoy and V. Corumlu, "Thermal performance of a thermosyphon heat pipe evacuated tube solar collector using silver-water nanofluid for commercial applications," *Renew. Energy*, vol. 122, pp. 26–34, Jul. 2018, doi: 10.1016/j.renene.2018.01.031.

[4] Y. Y. Gan, H. C. Ong, T. C. Ling, N. W. M. Zulkifli, C.-T. Wang, and Y.-C. Yang, "Thermal conductivity optimization and entropy generation analysis of titanium dioxide nanofluid in evacuated tube solar collector," *Appl. Therm. Eng.*, vol. 145, pp. 155–164, Dec. 2018, doi: 10.1016/j.applthermaleng.2018.09.012.

[5] M. A. Sharafeldin and G. Gróf, "Efficiency of evacuated tube solar collector using WO3/Water nanofluid," *Renew. Energy*, vol. 134, pp. 453–460, Apr. 2019, doi: 10.1016/j.renene.2018.11.010.

[6] M. A. Sharafeldin, G. Gróf, E. Abu-Nada, and O. Mahian, "Evacuated tube solar collector performance using copper nanofluid: Energy and environmental analysis," *Appl. Therm. Eng.*, vol. 162, p. 114205, Nov. 2019, doi: 10.1016/j.applthermaleng.2019.114205.

[7] M. I. Radwan, Gomaa, N. M. Elwekeel, and Abdelmagied, "Heating the air in buildings by evacuated tube solar collector used AL2O3/ water nanofluid at Cairo-Egypt climates," *Eng. Res. J.*, vol. 164, no. 0, pp. 229–249, Dec. 2019, doi: 10.21608/erj.2019.131383.

[8] A. Yurddaş, "Optimization and thermal performance of evacuated tube solar collector with various nanofluids," *Int. J. Heat Mass Transf.*, vol. 152, p. 119496, May 2020, doi: 10.1016/j.ijheatmasstransfer.2020.119496.
[9] M. Eltaweel, A. A. Abdel-Rehim, and A. A. A. Attia, "Energetic and exergetic analysis of a heat pipe evacuated tube solar collector using MWCNT/water nanofluid," *Case Stud. Therm. Eng.*, vol. 22, p. 100743, Dec. 2020, doi: 10.1016/j.csite.2020.100743.
[10] S. M. S. Hosseini and M. Shafiey Dehaj, "Assessment of TiO2 water-based nanofluids with two distinct morphologies in a U type evacuated tube solar collector," *Appl. Therm. Eng.*, vol. 182, p. 116086, Jan. 2021, doi: 10.1016/j.applthermaleng.2020.116086.
[11] İ. Özcan, A. Ozsoy, A. E. Özgür, and M. Karaboyaci, "An investigation of serial connected U-pipe evacuated tube solar collector performance using TiO2/Water nanofluid," *Appl. Therm. Eng.*, vol. 233, p. 121088, Oct. 2023, doi: 10.1016/j.applthermaleng.2023.121088.
[12] Y. A. Elmaboud, Kh. S. Mekheimer, and T. G. Emam, "Numerical Examination of Gold Nanoparticles as a Drug Carrier on Peristaltic Blood Flow Through Physiological Vessels: Cancer Therapy Treatment," *BioNanoScience*, vol. 9, no. 4, pp. 952–965, Dec. 2019, doi: 10.1007/s12668-019-00639-7.
[13] E. Azadian, S. Mousavi Ajarostaghi, M. Pourfallah, and M. Azadian, *Two-Dimensional Numerical Simulation of an Evacuated Tube Solar Collector by Finite Element Method*. 2019.
[14] M. Mercan and A. Yurddaş, "Numerical analysis of evacuated tube solar collectors using nanofluids," *Sol. Energy*, vol. 191, pp. 167–179, Oct. 2019, doi: 10.1016/j.solener.2019.08.074.
[15] A. Y. Sayed, S. I. Ahmed, K. S. Mekheimer, and M. S. Abdel-wahed, "Investigating the Impact of Magnetic Fields and Pulsating Pressure on Non-Newtonian Fluid Flow in Symmetric/Asymmetric Corrugated Microchannels," *Eng. Res. J.*, vol. 179, no. 0, pp. 43–67, Sep. 2023, doi: 10.21608/erj.2023.315737.
[16] M. S. Abdel-wahed, S. I. Ahmed, K. S. Mekheimer, and A. Y. Sayed, "Entropy generation analysis of a micropolar fluid in a corrugated channel with convective and slip conditions," *Case Stud. Therm. Eng.*, vol. 57, p. 104283, May 2024, doi: 10.1016/j.csite.2024.104283.
[17] A. Y. Sayed and M. S. Abdel-wahed, "Entropy analysis for an MHD nanofluid with a microrotation boundary layer over a moving permeable plate," *Eur. Phys. J. Plus*, vol. 135, no. 1, p. 106, Jan. 2020, doi: 10.1140/epjp/s13360-020-00181-6.
[18] M. S. Abdel-wahed and A. Y. Sayed, "Hybrid/mono-carbon nanotubes–water flow in a peristaltic curved channel with viscous dissipation," *Eur. Phys. J. Plus*, vol. 136, no. 9, p. 979, Sep. 2021, doi: 10.1140/epjp/s13360-021-01958-z.
[19] A. Y. Sayed, S. I. Ahmed, K. S. Mekheimer, and M. S. Abdel-wahed, "Electromagnetohydrodynamic effects with single-walled carbon nanotubes particles in a corrugated microchannel," *Chaos Solitons Fractals*, vol. 168, p. 113126, Mar. 2023, doi: 10.1016/j.chaos.2023.113126.
[20] W. Abbas, A. M. Megahed, M. A. Ibrahim, and A. A. M. Said, "Non-Newtonian Slippery Nanofluid Flow Due to a Stretching Sheet Through a Porous Medium with Heat Generation and Thermal Slip," *J. Nonlinear Math. Phys.*, vol. 30, no. 3, pp. 1221–1238, Sep. 2023, doi: 10.1007/s44198-023-00125-5.
[21] J.A. Duffie, W.A. Beckman, Solar Engineering of Thermal Processes, John Wiley & Sons, 2013.
[22] R. Tang, W. Gao, Y. Yu, and H. Chen, "Optimal tilt-angles of all-glass evacuated tube solar collectors," *Energy*, vol. 34, no. 9, pp. 1387–1395, Sep. 2009, doi: 10.1016/j.energy.2009.06.014.
[23] I. Budihardjo, G.L. Morrison, Performance of water-in-glass evacuated tube solar water heaters, Sol. Energy 83 (2009) 49–56.
[24] Y. A. Cengel, Heat and mass transfer: a practical approach, 2006.
[25] N. Sher Akbar, E. N. Maraj, N. F. M. Noor, and M. B. Habib, "Exact solutions of an unsteady thermal conductive pressure driven peristaltic transport with temperature-dependent nanofluid viscosity," *Case Stud. Therm. Eng.*, vol. 35, p. 102124, Jul. 2022, doi: 10.1016/j.csite.2022.102124.
[26] J. D. Anderson, "Governing Equations of Fluid Dynamics," in *Computational Fluid Dynamics: An Introduction*, J. F. Wendt, Ed., Berlin, Heidelberg: Springer, 1992, pp. 15–51. doi: 10.1007/978-3-662-11350-9_2.
[27] Y. He, Y. Men, Y. Zhao, H. Lu, and Y. Ding, "Numerical investigation into the convective heat transfer of TiO2 nanofluids flowing through a straight tube under the laminar flow conditions," *Appl. Therm. Eng.*, vol. 29, no. 10, pp. 1965–1972, Jul. 2009, doi: 10.1016/j.applthermaleng.2008.09.020.

[28] S. G. Elgendi, W. Abbas, A. A. M. Said, A. M. Megahed, and E. Fares, "Computational Analysis of the Dissipative Casson Fluid Flow Originating from a Slippery Sheet in Porous Media," *J. Nonlinear Math. Phys.*, vol. 31, no. 1, p. 19, Apr. 2024, doi: 10.1007/s44198-024-00183-3.
[29] A. N. Abdelsattar, A. A. El Desouky, A. A. Hammad, and M. S. Abdel-wahed, "Thermal analysis of MHD compressing fluid between two parallel disks exposed to linear and nonlinear thermal radiation supported by ternary nanoparticle: Analytical and numerical manipulation," *Nano*, Jul. 2024, doi: 10.1142/S1793292024501200.